Appendix

Photonic crystal lasers:

future integrated devices

5.1 Introduction

The technology of photonic crystals has produced a large variety of new devices. However, photonic crystals have not been integrated with mechanical structures or bottom-up nanomaterials. Both approaches have the potential to create novel devices.

The photonic crystal we have fabricated is a suspended slab of material. In a sense it already has a micromechanical aspect. The optical properties can be used with mechanical structures. The photonic crystal laser could be used for integrated optical detection of a nanoresonator beam. The principles of nanomechanical systems could also be used to improve the performance of the laser. For example, heating of the laser limits its performance. The periodic dielectric structure of the photonic crystal laser modifies not only the optical band structure, but also the phononic band structure. Engineering of both band structures simultaneously could increase the heat dissipation, allowing continuous wave lasing.

Photonic crystals can also be constructed out of bottom-up materials. Researchers have built microwave frequency waveguides using “log cabin” stacked dielectric rods.[1] However, it is a challenge to create these at optical frequencies. Metallic nanowires

could serve as the building blocks for such a structure. The hardest challenge of such an experiment is actually the fabrication of the device. Many possibilities for synergy exist between photonic crystals and nanomaterials.

5.2 Basics of photonic crystals

Photonic crystals utilize periodic changes in the index of refraction to engineer the band structure for electromagnetic waves. They have been an extremely active area of research since the pioneering work of Yablonovitch.[2] Photonic crystals have been utilized to create a variety of light trapping devices such as waveguides[3], lasers[4], and optical cavities for cavity quantum electrodynamics.[5] Research is currently underway to apply photonic crystals to diverse fields from atom trapping[6] to chemical sensing.[7] Groups have also fabricated photonic crystal optical fiber[8], some of which trap light in air, rather than dielectric.

The electronic band gap that arises in crystal lattices of atoms is a well known phenomenon that has yielded the incredible advances in computing of the later 20th century. An analogous effect exists with regard to photons. By constructing a periodic lattice of contrasting index of refraction, one can create a material with a photonic band gap, where certain frequencies of light are forbidden from propagating through the material. So called “photonic crystals” have the potential to lead another revolution in information processing, where electrons are replaced by photons. The photonic bands that lie above and below the gap can be referred to, in analogy to solid state physics, the “conduction” band and the “valence” band, respectively.

Photonic crystals have been constructed with band gaps in one, two and three dimensions.[9] The Bragg mirror is an early incarnation of a photonic band gap structure, used to reflect a specific wavelength of light. The mirror is constructed by stacking alternating layers of two materials with different indices of refraction. Each layer has a thickness corresponding to ¼ of the wavelength of the light to be reflected. The constructive and destructive interference of the reflections off of each layer prevent the corresponding wavelength from propagating. The "quarter-wave stack" forms the basis for devices such as the Fabry-Perot filters and distributed feedback lasers.

Maxwell's equations, the basic laws that describe the propagation of light, are scalable in the absence of free charges and currents. Therefore, in theoretical analysis of photonic crystals it is common to normalize physical dimensions by the lattice spacing of the photonic crystal *a*. In this chapter we will refer to the normalized hole radius *r/a* and the normalized slab thickness *d/a* when considering the design and tuning of the device. In addition, a normalized frequency can also be defined,

$$\omega^n = \frac{a\omega}{2\pi c} = \frac{a}{\lambda_0}$$

where ω is the angular frequency, c is the speed of light, λ_0 is the wavelength in vacuum. For fixed normalized dimensions, the wavelength scales with the lattice spacing.

5.3 Design

There are several ways to analyze the behavior of light in periodic structures including solving an electromagnetic master equation[10] and using plane wave

expansion.[11] Another common method is the use of finite-difference time-domain (FDTD) simulation.[12] In an FDTD calculation the spatial and time dimensions are discretized with a fine mesh. Then at each time step the electric and magnetic field and their time derivatives are calculated. This process is iterated to yield the propagation of electromagnetic radiation through the crystal. All the calculations presented here were performed by Dr. Oskar Painter, a senior graduate student at the time.

The microcavity studied here is formed from two basic building blocks: a dielectric slab and a 2-D photonic crystal. The slab provides in-plane confinement through total internal reflection. The photonic crystal alters the propagation of light, with certain frequencies that cannot propagate through the periodic structure. Since the slab is only about half a wavelength thick, the finite thickness of the 2-D photonic crystal must be taken into account.

The 2-D lattice employed in this work is a triangular lattice of air holes in a dielectric material. An ideal 2-D photonic crystal with infinite thickness has modes which can be classified transverse electric (TE) or transverse magnetic (TM), where the electric or magnetic field, respectively, is parallel to the 2-D plane of the photonic crystal lattice.[13] For a finite thickness 2-D photonic crystal the modes are classified even or odd, with respect to the horizontal mirror plane in the center of the slab. For the lower lying bands of the ideal lattice, the even and odd modes guided by the slab may be termed TE-like and TM-like, respectively.[14]

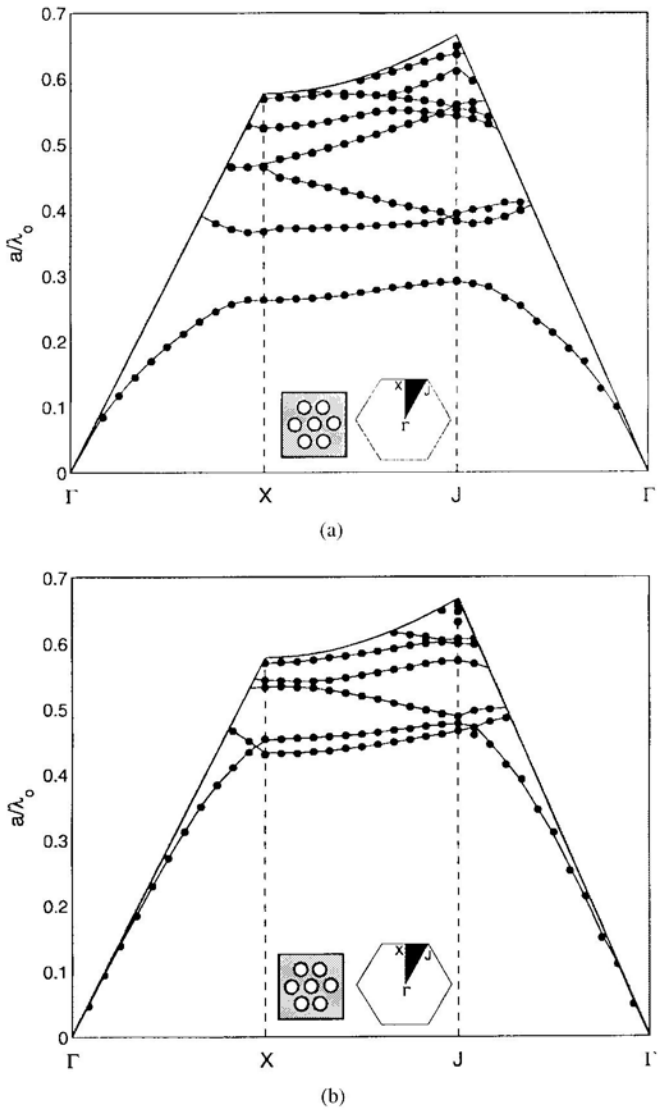

Figure A.1: In-plane band structure of triangular lattice of air holes in a dielectric slab. (a) TE-like modes (b) TM-like modes The parameters used to calculate these band diagrams are r/a = 0.32, d/a = 0.409, n_{slab} = 3.4 and n_{air} = 1.

The in-plane band structure of the triangular lattice photonic crystal is shown in Figure A.1, computed by FDTD simulation. The parameters used in this calculation are: r/a = 0.32, d/a = 0.409, n_{slab} = 3.4 and n_{clad} = 1. The shaded regions in the plots of Figure A.1 are above the light line of photons in the air cladding. Photons with

wavelength and in-plane *k*-vector above the light line can propagate in air, so that these modes are leaky modes. The bands plotted below the light line represent guided modes of the photonic crystal. Comparing the allowed modes in Figures 1a and 1b, we can see that the TE-like modes have a photonic band gap at certain normalized frequencies around 0.3 while the TM-like modes have no band gap. This is favorable for the purposes of creating a defect laser cavity, for it reduces the number of high Q modes, decreasing the threshold for lasing.

The band gap for TE-like modes results in a range of optical frequencies which cannot propagate through the photonic crystal. By removing a single air hole from the center of a triangular lattice, a defect is formed which acts as a potential well and resonant cavity for photons. The photonic crystal surrounding the resonant cavity acts as a mirror for wavelengths within the band gap. Figure A.2 shows a schematic of the device. The power that is radiated in the form of photons from the defect cavity can be divided into a component that escapes out vertically from the slab and a component that tunnels through the finite periods of the photonic crystal. The latter leakage can be improved by adding layers to the lattice, till scattering and absorption begin to dominate the losses. The photons that leak vertically from the waveguide impose a greater limitation on the *Q* factor of the cavity. Smaller air holes increase the effective index of the slab, improving in-plane confinement. The *Q* calculated from FDTD simulation for the devices studied here is 500-600.

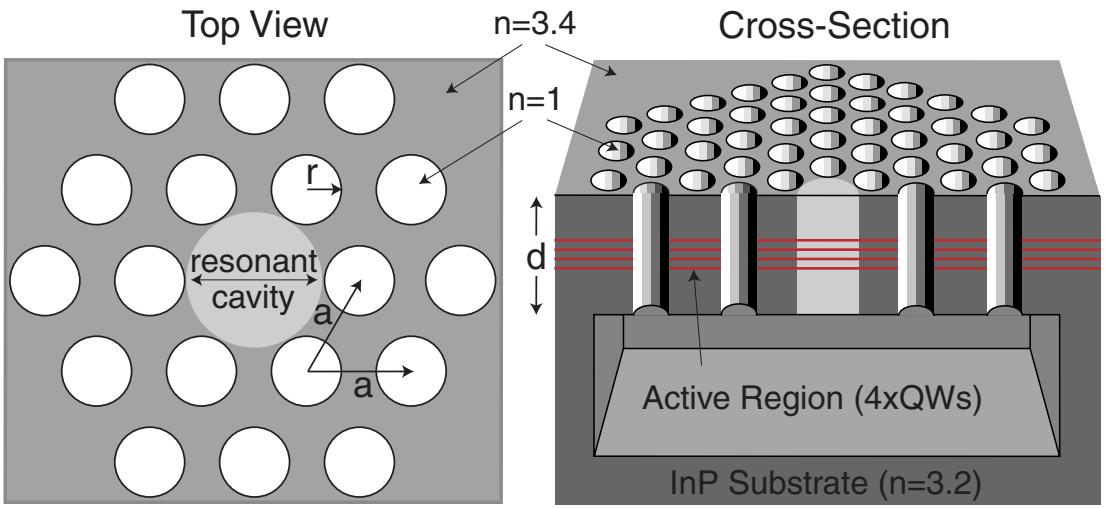

Figure A.2: Left—top view of photonic crystal defect laser showing triangular lattice and cavity with missing hole. Right—cross section of device showing suspended structure and quantum wells for optical gain.

To create a structure that exhibits lasing, there are two main components: a high-Q optical cavity and an optical gain material. The optical medium selected for this device is eptiaxially grown III-IV semiconductor material with quantum wells. Electron-hole pairs are excited by optical pumping. The quantum wells provide a region where electron-hole recombination can emit photons into the cavity modes. Details of the epitaxy can be found in Section 5.5.

5.4 Tuning

The effects of the in-plane confinement on the wavelength of cavity modes can be approximated by separating the in-plane and vertical components of momentum,

$$\omega^2 \approx \omega_{2D}^2 + \left(\frac{c}{n_{eff}^z}\right)^2 k_z^2$$

where ω_{2D} is the in-plane frequency of the confined mode, $k_z = 2\pi/\lambda_z$ is the wavevector corresponding to the vertical confinement, and n^z_{eff} is the effective index determined by the overlap between the perforated slab and the field pattern of the 2D mode. The fundamental guided mode of a dielectric slab, for strong confinement, has $\lambda_z = 2d$. Substituting into equation (2) and normalizing as proscribed by equation (1), we find

$$\omega^n \approx \sqrt{\left(\omega^n_{2D}\right)^2 + \left(\frac{1}{2n^z_{eff}}\right)^2 \left(\frac{d}{a}\right)^{-2}} \quad .(1)$$

For the defect cavities fabricated in this work, the thickness d is constant. Therefore with constant r/a, the normalized frequency will increase with increasing lattice spacing a.

The change in the in-plane frequency component with r/a is more complicated due to its effect on the band structure of the crystal. It can be argued that as r/a increases, the frequency increases due to the reduced fraction of dielectric material. In this work we vary the parameters a, d/a and r/a to measure their effect on the photonic crystal defect modes.

5.5 Fabrication

The geometry of this device is a perforated slab of optical semiconducting material. The material must provide the light emission which will be trapped in the photonic crystal defect cavity. This is achieved by the presence of quantum wells. In addition, the material must have low surface recombination of electrons and holes. Surface recombination is not light emitting, so it reduces the pumping efficiency of the device. This process is particularly important because the geometry of this device results

in a large surface area to volume ratio. Light is trapped in-plane by total internal reflection, which is maximized by having air cladding on both sides of the slab. To create a suspended slab of material, a sacrificial layer is included.

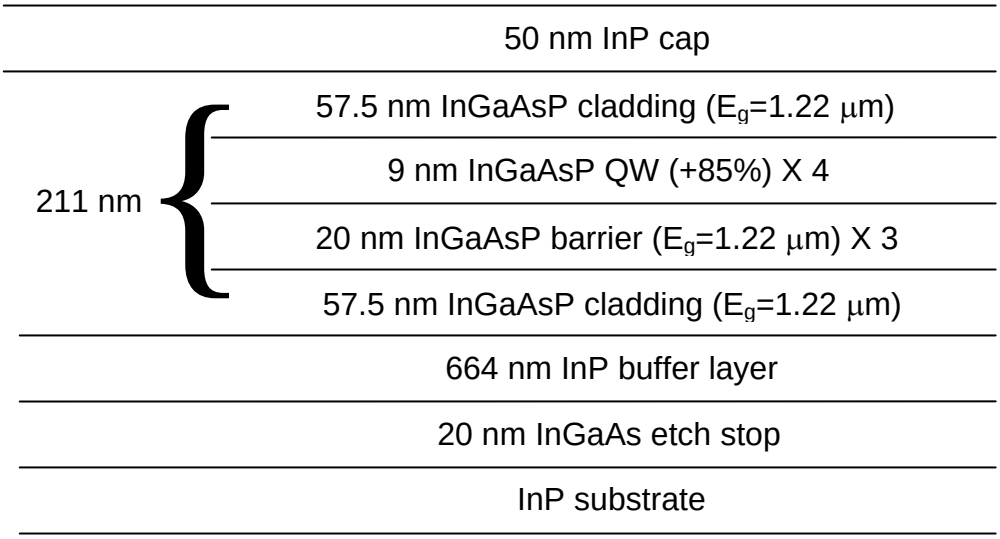

Figure A.3: Schematic of epitaxial layers for defect lasers.

Figure A.3 depicts the epitaxial layers of the wafer used to fabricate this device. Collaborators J. D. O'Brian and P. D. Dapkus at USC used metal-organic chemical vapor deposition (MOCVD) to grow the epitaxial layers on an InP substrate. Going up from the InP substrate, the epitaxy contains a thin InGaAs etch stop layer, InP sacrificial layer, four quantum wells with barrier layer, and finally a InP cap. The quantum wells are comprised of 0.85% compressively strained InGaAsP layers with peak emission at 1.55μm. The barriers between the quantum wells are also InGaAsP with a bandgap corresponding to photons of wavelength 1.22μm. Two cladding layers identical to the barrier layers surround the quantum wells, further isolating them from the surface and

increasing the total thickness of the final device. The InP buffer layer will be etched away to leave a suspended slab structure at the end of the fabrication.

A series of mask layers is used to transfer a perforation pattern through the active region to the InP sacrificial layer. Electron beam lithography defines the pattern in a 100 nm resist layer of 2% polymethyl methacrylate (PMMA). Argon ion beam etch transfers the pattern to an underlying metal layer of Cr/Au. Next, a C_2F_6 reactive ion etch (RIE) is used to etch the holes into a SiO_2 layer. The final dry etch step is a Cl_2 chemically assisted ion beam etch (CAIBE) that perforates the optical material through to the InP sacrificial layer. To suspend the patterned slab, the InP sacrificial layer must be reomoved. A gently agitated hydrochloric acid (4:1) solution is used to selectively etch away the InP, leaving the photonic crystal structure surrounded by air.

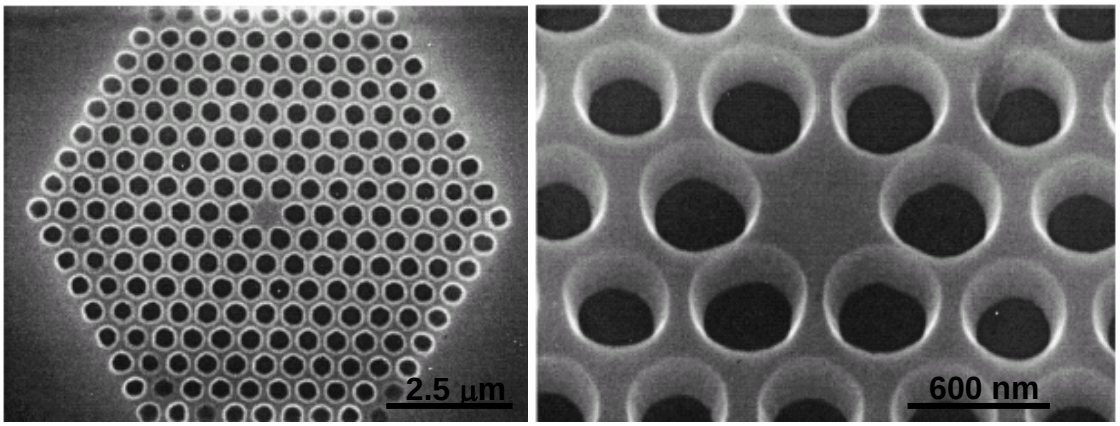

Figure A.4: Left—completed photonic crystal. Right—detail of defect area of device.

SEM images of completed devices is shown in Figures 4 and 5. The fabrication process results in a suspended slab of optical material perforated with a triangular lattice of holes 8 periods deep surrounding a single missing hole in the center. We fabricated an

array of devices varying the lattice constant *a* and the hole radius *r*, shown in Figure A.5. The average diameter of each device was about 8 mm and they were space by 10 mm. The lattice constant is varied from 564 nm to 470 nm and the normalized hole radius *r/a* for each lattice spacing is varied from 0.30 to 0.37.

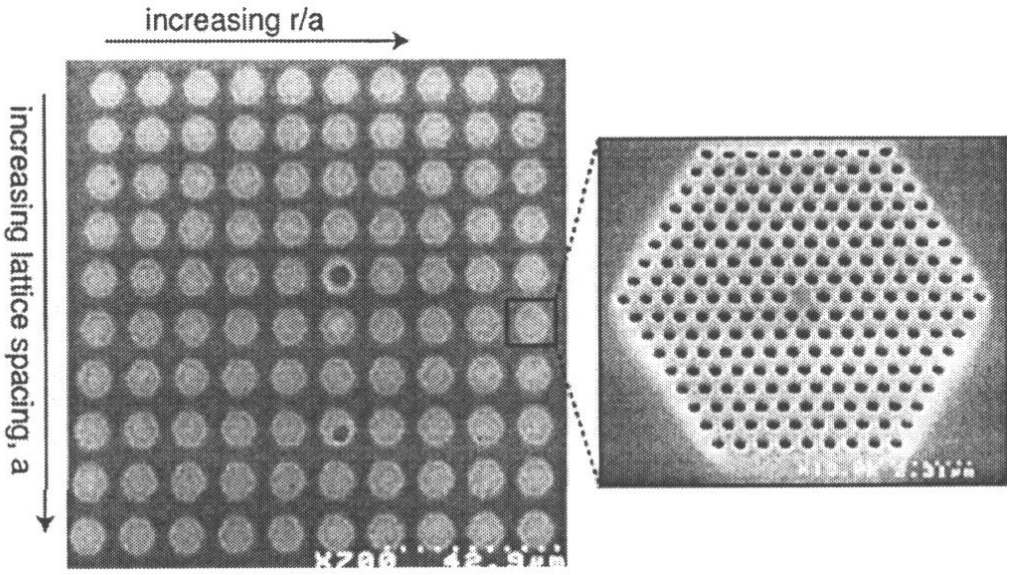

Figure A.5: Array of photonic crystal devices with magnification of one device. The lattice constant is varied from 564 nm to 470 nm and the normalized hole radius *r/a* for each lattice spacing is varied from 0.30 to 0.37.

5.5 Measurement

To pump this structure, electrons within the quantum wells must be excited to the conduction band. They then relax to the valence band, emitting light of a frequency corresponding to the band gap of the quantum well. If the defect mode of the cavity has

the same frequency, the light will resonate in the defect cavity. If the cavity Q is high enough, the trapped light will cause stimulated emission from the quantum wells, resulting in lasing.

The sample was mounted on an X-Y-Z stage and illuminated with light from an 830 nm semiconductor laser diode at a normal incidence. A high numerical aperture, long working distance 100X lens is used to image the devices, focus the pump light and collect the resulting photoluminescence (PL). The spot size of the beam can be focused down to 1 μm, though a 4 μm spot size provided the lowest lasing threshold. This is because a larger spot size pumps the surrounding quantum wells in the photonic crystal to transparency so that they doesn't absorb the evanescent light from the defect mode. A spot size of 4 μm was used throughout this work. The collected light is filtered by a GaAs wafer to remove the pump beam and then fed into an optical spectrum analyzer (OSA).

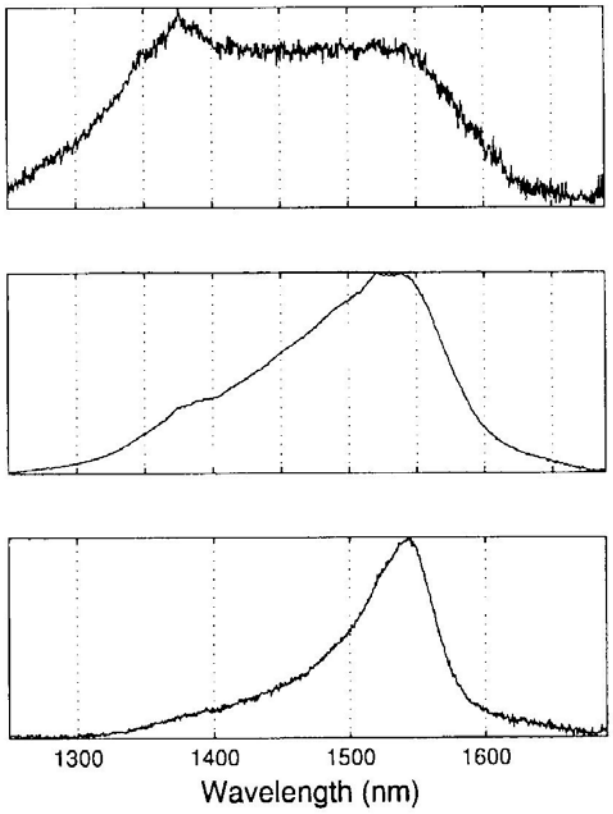

Figure A.6: Photoluminescence at three pump powers for an unpatterned area on the substrate with 4 mm spot size. The bottom plot corresponds to 20 μW continuous wave pump power. The middle plot is 170 μW pump power with a 50% duty cycle. The top plot is the PL for 7 mW peak pump power with 10 ns pulses and 3 μs period, the same pumping as used for testing the defect cavity lasers.

We first pumped and collected at an unprocessed, unpatterned area of the sample to measure the PL in the absence of photonic crystal, plotted in Figure A.6. The peak pump power is increased from bottom to top in Figure A.6. At low pump power the peak emission is at 1545 nm corresponding to the lowest energy level in the quantum wells, as shown in the bottom plot of Figure A.6. At higher pump power, shown in the middle plot, another peak at 1380 nm appears, corresponding to the first excited state of the

quantum well. At pumping conditions identical to those used for these experiments (7 mW peak power, (10 ns pulse with a 3 μs period) the PL is quite broad covering almost a 400 nm range, as shown in the top plot of Figure A.6. The broadening arises due to heating of the substrate at high pump power. The broadening is useful in that it expands the range of frequencies that the quantum wells will emit into, though heating also increases the amount of non-radiative recombination of electrons and holes.

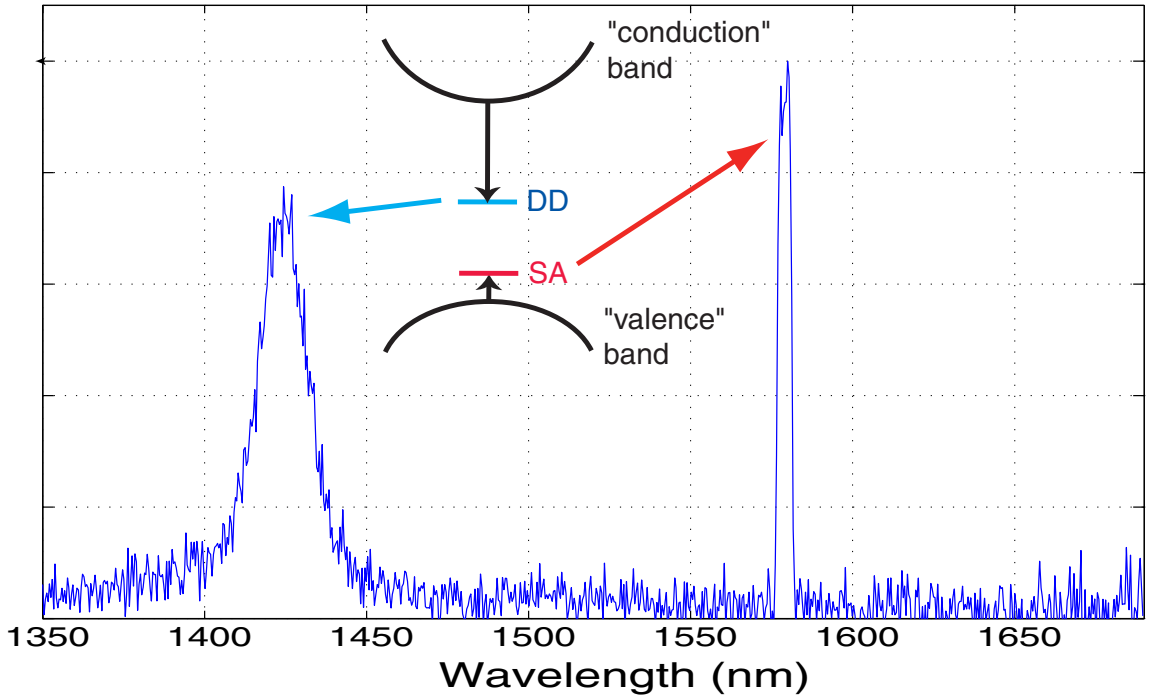

Figure A.7: Sub-threshold photoluminescence from a typical photonic crystal defect cavity.

The PL from the photonic crystal defect cavity devices was markedly different. Figure A.7 shows the PL from a typical device. The photonic crystal suppresses emission into the photonic band gap except for two resonance peaks that correspond to defect

cavity modes. The inset shows a schematic of the band structure showing where the two modes lie relative to the photonic band gap. The longer wavelength mode at 1580 nm corresponds to a weakly localized shallow "acceptor" (SA) mode, while the other is a strongly localized pair of degenerate deep "donor" (DD) modes at 1425 nm.

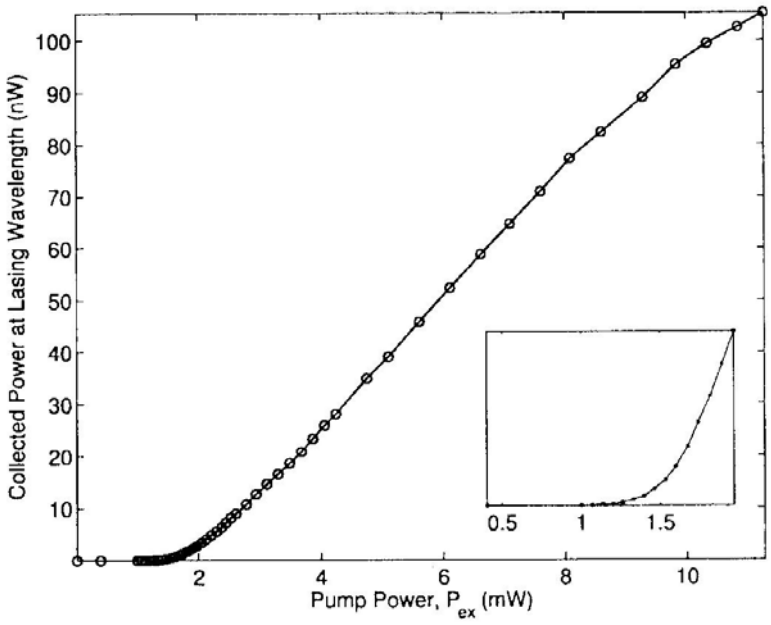

Figure A.8: Collected lasing optical power at 1580 nm vs. external peak pump power of a defect cavity device.

Each device was tested for lasing by pumping it with the diode laser at 7 mW peak pump power with 10 ns pulses and 3 μs period. The lasing from each defect cavity was always the longer wavelength SA mode, due to a theoretical Q five times that of the DD modes. The collected light power is plotted versus the peak pump power to show the lasing threshold. The inset gives a magnified plot of the "knee," showing that the threshold pump power is 1.5 mW, from which we estimate an absorbed power of 500 μW due to reflections from the lens and sample surface. Lasing was obtained for duty cycles of up to 1%, corresponding to a 30 ns pulse. Lasing at higher duty cycles does not occur probably because of heating in the suspended membrane. The membrane is poorly heat

sunk so that nonradiative Auger recombination, which increases exponentially with temperature, consumes the excited electrons and holes in the quantum well.

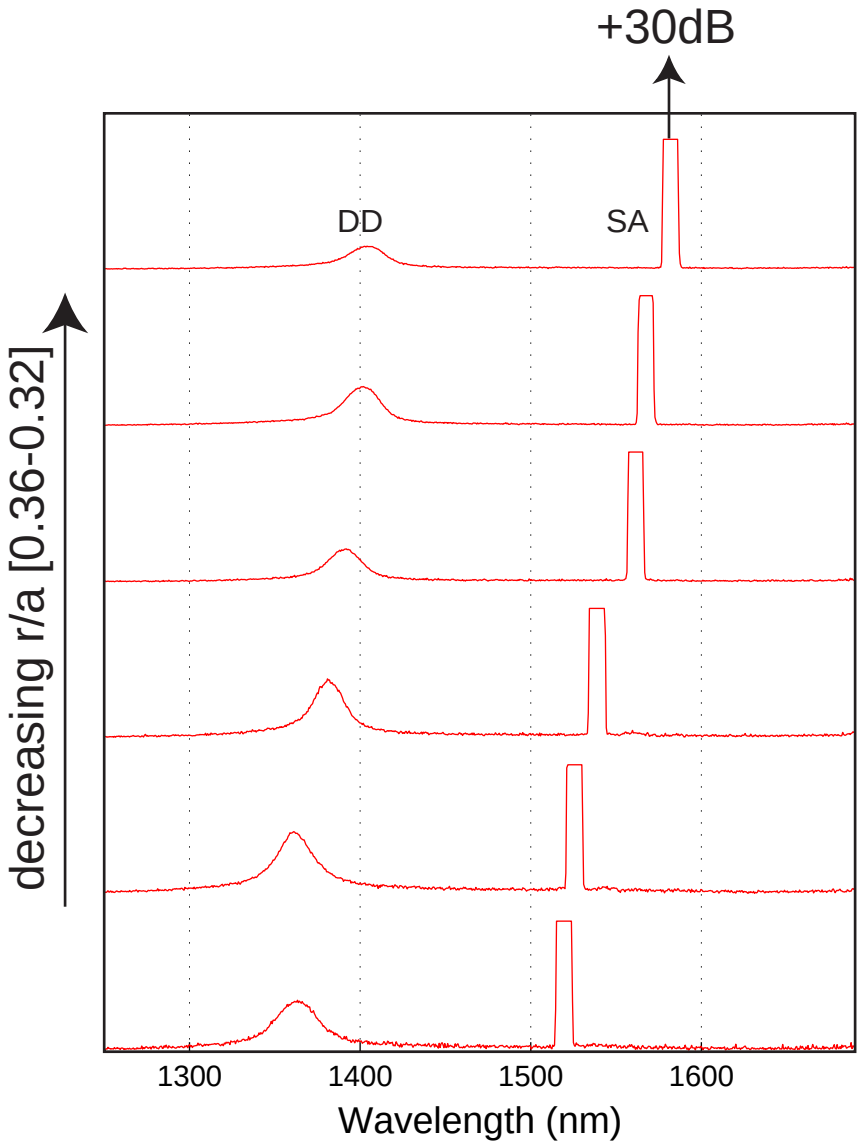

Figure A.9: Photoluminescence from a set of defect cavities, showing tuning as a function of *r/a*. The lattice spacing in this case is 490 nm while the radius of the air holes ranges from 165 nm to 150 nm.

The PL for a set of devices with constant lattice spacing of 490 nm and r/a that varies from 0.36 to 0.32 is shown in Figure A.9. As the normalized hole radius is

decreased both the SA and DD modes increase in wavelength as expected. The lasing wavelength of the SA modes can be tuned lithographically from 1520 nm to 1580 nm. The lasing wavelength increases by about 10 nm for a reduction of the diameter of the air holes by about 5 nm, close to the resolution of our lithography.

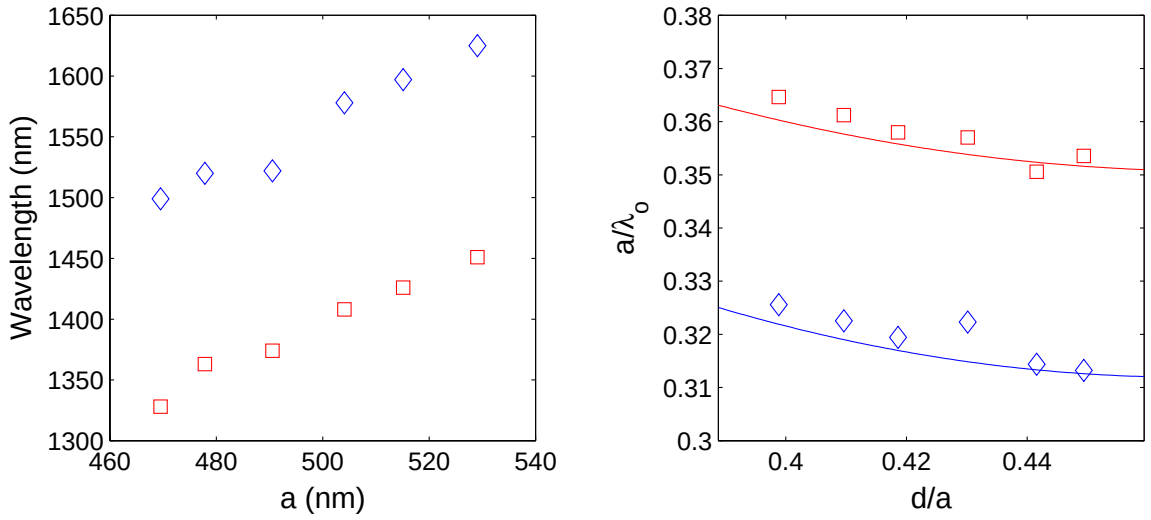

Figure A.10: Left—emission wavelength for SA laser peak (diamonds) and DD peak (squares) for increasing lattice spacing. Right—SA and DD wavelengths for normalized slab thickness. The lines plot FDTD simulations of the SA and DD mode frequency.

If the normalized hole radius *r/a* is held constant at 0.35, then varying the lattice constant will vary the normalized slab thickness *d/a*. Figure A.10 plots the wavelength of the SA and DD photoluminescence peaks as a function of the lattice constant, and in the right graph, plots the corresponding normalized frequency a/λ_0 versus *d/a*, both for fixed *r/a*. Due to the scaling of Maxwell's equations, the wavelength increases with *a* as expected. Also, the normalized frequency decrease slightly with increasing *d/a* as predicted by equation (1). The dashed curves in the right plot of Figure A.10 show the

theoretical predictions of the locations of the SA and DD from FDTD simulation which agree well with the measured data.

5.6 Summary

Photonic crystals can be used to create high-Q optical cavities. By adding a gain medium to the structure a laser can be constructed. We have constructed a laser of wavelength about 1.55 μm from a suspended perforated optical slab. The slab is perforated with a triangular lattice of circular air holes. The frequency of the lasing mode can be tuned over 150 nm by varying the lattice spacing, hole radius or slab thickness. Integration of photonic crystals with nanowires and other nanomechanical devices has the potential for revolutionary devices.

References

[1] E. Ozbay, B. Temelkuran, M. Sigalas et al., "Defect structures in metallic photonic crystals," *Applied Physics Letters* **69** (25), 3797-3799 (1996).

[2] E. Yablonovitch, "Inhibited spontaneous emission in solid-state physics and electronics," *Physical Review Letters* **58** (20), 2059-2062 (1987).

[3] M. Loncar, J. Vuckovic, and A. Scherer, "Methods for controlling positions of guided modes of photonic-crystal waveguides," *Journal of the Optical Society of America. B, Optical Physics* **18** (9), 1362-1368 (2001).

[4] M. Loncar, M. Hochberg, A. Scherer et al., "High quality factors and room-temperature lasing in a modified single-defect photonic crystal cavity," *Optics Letters* **29** (7), 721-723 (2004).

[5] J. Vuckovic, M. Pelton, A. Scherer et al., "Optimization of three-dimensional micropost microcavities for cavity quantum electrodynamics," *Physical Review. A* **66** (2), art.no.-023808 (2002).

[6] J. Vuckovic, M. Loncar, H. Mabuchi et al., "Design of photonic crystal microcavities for cavity QED," *Physical review. E, Statistical Physics, Plasmas, Fluids, and Related Interdisciplinary Topics* **6501** (1), art.no.-016608 (2002).

[7] M. Loncar, A. Scherer, and Y. M. Qiu, "Photonic crystal laser sources for chemical detection," *Applied Physics Letters* **82** (26), 4648-4650 (2003).

[8] J. C. Knight, J. Broeng, T. A. Birks et al., "Photonic band cap guidance in optical fibers," *Science* **282** (5393), 1476-1478 (1998).

[9] J. G. Fleming, S. Y. Lin, I. El-Kady et al., "All-metallic three-dimensional photonic crystals with a large infrared bandgap," *Nature* **417** (6884), 52-55 (2002).

[10] R. D. Meade, K. D. Brommer, A. M. Rappe et al., "Electromagnetic Bloch waves at the surface of a photonic crystal," *Physical Review. B, Condensed Matter* **44** (19), 10961-10964 (1991).

[11] H. S. Sozuer, J. W. Haus, and R. Inguva, "Photonic bands: Convergence problems with the plane-wave method," *Physical Review. B, Condensed Matter* **45** (24), 13962-13972 (1992).

[12] P. R. Villeneuve, S. H. Fan, and J. D. Joannopoulos, "Microcavities in photonic crystals: Mode symmetry, tunability, and coupling efficiency," *Physical Review. B, Condensed Matter* **54** (11), 7837-7842 (1996).

[13] J. D. Joannopoulos, Robert D. Meade, and Joshua N. Winn, *Photonic crystals: molding the flow of light*. (Princeton University Press, Princeton, N.J., 1995), pp.ix, 137.

[14] P. R. Villeneuve, S. Fan, S. G. Johnson et al., "Three-dimensional photon confinement in photonic crystals of low-dimensional periodicity," *IEE Proceedings. Optoelectronics* **145** (6), 384-390 (1998).